Journal of Materials Chemistry A

Accepted Manuscript

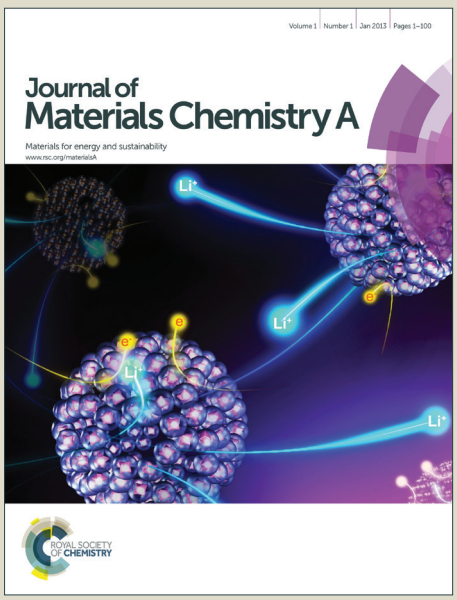

ROYAL SOCIETY OF CHEMISTRY

www.rsc.org/materialsA

Electrocatalytic property of vertically oriented graphene film and its application as catalytic counter electrode for dye-sensitized solar cells

Xuan Pan[1], Kai Zhu[2*], Guofeng Ren[1], Nazifah Islam[1], Juliusz Warzywoda[3], Zhaoyang Fan[1]*

[1]Department of Electrical and Computer Engineering and Nano Tech Center, Texas Tech University, Lubbock, Texas, 79409, USA; [2]Chemical and Materials Science Center, National Renewable Energy Laboratory, Golden, Colorado 80401, USA; [3] Materials Characterization Center, Whitacre College of Engineering, Texas Tech University, Lubbock, Texas, 79409, USA

*Email: kai.zhu@nrel.gov; zhaoyang.fan@ttu.edu

ABSTRACT

Vertically-oriented graphene (VOG), with graphene sheets perpendicular to the substrate, exhibits meritorious electrocatalytic properties due to the fully exposed graphene (or graphitic) edges and other plasma introduced defects, even without any heteroatom functionalization. We report the growth and electrocatalytic properties of VOG by plasma-enhanced chemical vapor deposition using methane and nitrogen as source gases. Nitrogen was adopted as plasma ancillary gas to obtain higher plasma temperature that promotes VOG growth with better electrocatalytic performance, as comparative studies demonstrated. Electron transfer dynamics measurement using $Fe(CN)_6^{3-/4-}$ redox couple found reduction and oxidation peak-to-peak separation as low as 70 mV, indicating rapid electron-transfer kinetics. The electrocatalytic activity of VOG electrode on I^-/ I_3^- redox couple was found approaching that of platinum. Using VOG as counter electrode for dye-sensitized solar cells (DSSCs), a promising power conversion efficiency of 7.63% was demonstrated. Electrochemical impedance spectroscopic study further discloses the impact of VOG property on DSSC performance.

1. Introduction

The development of sustainable technologies requires minimizing the consumption of precious materials, and this is especially true for the development of cost-effective dye-sensitized solar cell (DSSC),[1] a promising alternative to the semiconductor p-n junction based photovoltaic devices. Although photoanode is the most critical component of a DSSC to determine the device efficiency, and has been under extensive investigation,[2-8] the issues related to the platinum-based cathode must also be addressed. A typical design of DSSC consists of a mesoporous TiO_2 photoanode sensitized by dye molecules, a counter electrode (CE) as cathode, and iodide-triiodide (I^-/I_3^-) redox pair based electrolyte. After interfacial electron injection from photo-excited dye molecule into TiO_2, the sensitizer must be regenerated through electron donation from neighboring I^-/I_3^- redox pair as a mediator; subsequently, the oxidized iodide ion diffuses to the CE and is catalytically reduced by acquiring an electron passing through the external circuit from the photoanode. Since the CE determines the reduction rate of the I^-/I_3^- redox pairs, which further determines the regeneration rate of dye molecules, a material with high reduction activity is essential for the CE. Ideally, this material should possess a large surface area with enough active sites, low reduction overpotential and high electronic conductivity to minimize potential loss, and chemical stability for long device lifetime. Nanoparticulate platinum film has been used for this purpose to achieve highly efficient DSSCs. However, substitution of platinum with earth abundant materials is essential for the development of sustainable and cost-effective DSSC technology. To this end, a variety of carbonaceous nanomaterials has been actively investigated[9-12].

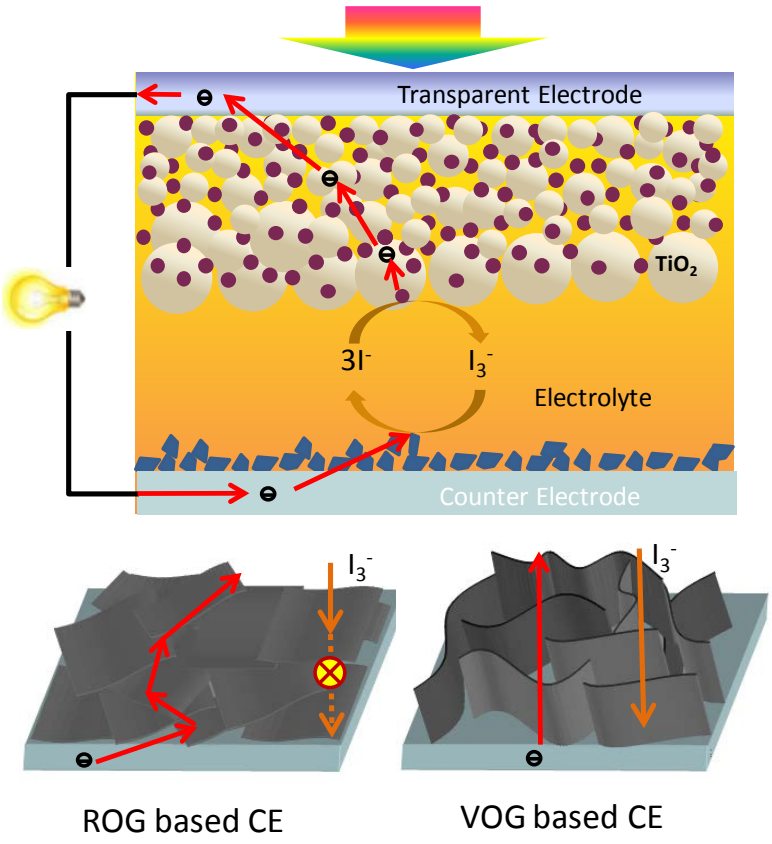

Figure 1. Schematic comparing laterally oriented graphene (LOG) with vertically oriented graphene (VOG) based counter electrodes for DSSC.

Graphene, due to its sharp edges with active bonds or intentionally functionalized in-lattice or out-of-plane heterobonds, possesses strong catalytic activity. It is generally argued that due to the large surface area with high-density active sites, high electronic conductivity, in addition to the abundance and chemical stability of carbon, graphene might be a promising candidate as the counter electrode material for DSSCs.[13] In particular, the application of reduced graphene oxide (RGO) sheets, due to easier production through liquid phase exfoliation, as the CE of DSSCs has been drawing considerable attentions in recent years.[14] However, the progress is not satisfactory considering that the resultant DSSC has a much smaller fill factor (FF) and hence a lower conversion efficiency when comparing with cells using Pt-based CEs.[15] This may

be understood based on the following reasoning: 1) the catalytic activity of RGO comes from oxygen-related bondings, while these heterbonds significantly diminish the electronic conductivity of graphene. A compromise must be made between conductivity and catalytic activity; 2) during drying of the randomly stacked RGO sheets formed by liquid phase exfoliation, the surface tension of the retreating liquid meniscus causes individual sheet structure collapse into "bulk" structure, significantly reducing surface area and active sites; 3) the superior electron transport property of graphene lies in its 2D plane, while in the electrode formed by laterally oriented graphene (LOG), electron must transport in the perpendicular out-of-plane direction, leading to a significant resistive loss; 4) the lateral orientation further blocks ion transport in the perpendicular direction from accessing the catalytic active sites on those RGO sheets lying in the deep; 5) long-term mechanical stability of the electrode is in question if binder, which is highly resistive, is not used; 6) contact resistance between graphene sheets and metallic foil support is another issue. Although employing mixtures of RGO with other nanoparticles or nanowires[16] or other composite[17] may partially relieve these restrictions, an optimized approach to the design of graphene based electrodes in general, and the CE for DSSC in particular, is greatly demanding. Very recently, new format of graphene based electrodes, such as graphene nano-foam,[18] nitrogen-doped graphene foam,[19, 20] graphene aerogel,[21] 3D honeycomb-like structured graphene,[22] have been reported to overcome the several issues related to the LOG structure. Vertically-oriented multilayer graphene (VOG) film, directly deposited on a metallic foil by plasma enhanced chemical vapor deposition (CVD), is another format of graphene and it does not contain oxygen heteroatom.[23] VOG has attracted great attention to develop ultrafast electrical double layer capacitors to work at hundreds to kilohertz frequencies.[24, 25] It is interesting to investigate its capability as CE of DSSC to overcome the above limitations of LOG based CE. To this end, we

report the electrochemical study and DSSC performance using VOG films as CE for high performance DSSC. Fig. 1 schematically compares electron and ion transport paths in LOG and VOG based CEs. It is clear that the above limitations related to LOG based electrode can be eliminated by VOG electrode. The large electronic conductivity of VOG in its vertical sheet facilitates fast charge transport with minimum potential loss. VOG also possesses a large surface area to provide abundant active sites and a straightforward porous geometry to offer fast mass transfer of the redox species, essential for fast redox reaction. These merits of VOG ensure achieving an electrode with high electronic conductivity, facilitating ion transport and increasing the density of catalytic active sites, which will minimize potential loss, provide high rate iodine reduction for fast regeneration of dye molecules, and hence lead to a high power conversion efficiency.

In this work, VOG films were deposited on molybdenum (Mo) foils in a microwave plasma CVD (MPCVD) reactor with CH_4 and N_2 as source gases. Due to the very high growth temperature (> 1200^{o}C), nitrogen atoms were not incorporated into the VOG lattice. Unlike the previous reports that the catalytic reduction of the I^-/I_3^- redox pairs of graphene or RGO is mainly related to nitrogen or boron doping or oxygen-containing functional groups,[18, 19, 21, 26, 27] our VOG films, without intentional dopants or functional groups, possess the catalytic function mainly due to the fully exposed sharp edge planes and other in-plane defects.[23]

2. Experimental Section

VOG film preparation: a 1.5 kW microwave plasma CVD system from Seki Technotron was used for VOG sample deposition. It was found that a high substrate temperature (> 1200^{o}C) is essential to achieve a high growth rate and a quasi-vertical sheet morphology, and therefore molybdenum (Mo) foil was selected as the substrate for VOG deposition in a gas mixture of

methane and nitrogen. Introduction of nitrogen gas can significantly increase plasma temperature. In order for the substrate to be directly heated to high temperature by plasma heating, a thermal-insulating pedestal was used to lift up the 15 mm x 15 mm Mo substrates from the water-cooled substrate holder. All the source gases used, including CH_4, N_2, and H_2, have a purity of 99.999%, with H_2 gas further passed through a palladium-based hydrogen purifier. Prior to growth, the substrate heater temperature was ramped up and maintained at 650 ^oC. The substrate was cleaned using hydrogen plasma for 5 minutes with a hydrogen flow rate of 300 sccm, a chamber pressure of 30 torr, and a microwave power of 1 kW. After that, the growth was carried out at a microwave power of 1 kW and a pressure of 45 torr in a gas mixture of methane and nitrogen, with methane flow rate of 50 sccm and a variable nitrogen flow rate of 100, 200, and 300 sccm. Correspondingly, the samples grown under these different nitrogen flow rates are called S1, S2, and S3. During the growth, the substrate heater was maintained at 650^oC, however, since Mo substrate was sit on a thermal-insulating pedestal and intruded into plasma, accurate substrate temperature was unknown. However, it did increases as nitrogen flow rate was ramped up since higher nitrogen flow strongly increased plasma intensity. All growth lasted 30 minutes.

C*haracterizations*: The morphology of vertically oriented graphene was characterized by a field-emission scanning electron microscope (SEM). Raman spectra were recorded by a Bruker SENTERRA dispersive Raman microscope spectrometer with excitation laser beam wavelength of 532 nm. The chemical composition and bonding states were studied using a PHI 5000 VersaProbe X-ray photoelectron spectrometer (XPS).

Electrochemical measurements: Electrochemical study was carried out using an electrochemical workstation at room temperature. The electron-transfer dynamics study between VOG films and electrolyte was conducted using $Fe(CN)_6^{3-/4-}$ redox couple by cyclic voltammetry

in an electrolyte of 0.1 M KCl aqueous solution containing 0.25 mM $K_3[Fe(CN)_6]$ / $K_4[Fe(CN)_6]$ (1:1). To investigate the electrocatalytic activity of VOG electrode as to I^-/ I_3^- redox couple, cyclic voltammogram of VOG electrode was measured in acetonitrile solution containing 10 mM LiI, 1 mM I_2 and 0.1 M $LiClO_4$. A three electrode configuration was employed with Pt wire as the counter electrode and non-aqueous reference electrode (ANE) as the reference electrode. The custom-made non-aqueous Ag/Ag^+ reference electrode consists of glass tubing with a porous Teflon tip and a Teflon cap with a silver wire. Acetonitrile (anhydrous, 99.8%, Sigma-Aldrich) containing 0.01 M silver nitrate was prepared to fill the compartment (both the glass tubing and the Teflon cap). To assemble the ANE, air bubble trapped in the tubing was removed, and then the glass tubing was slowly inserted into the cap with a silver wire. The potential of the custom-made ANE was calibrated in a bulk solution made from the acetonitrile containing 2.5 mM ferrocene redox couple supported by 0.1 M tetrabutylammonium perchlorate (TBAP). A three electrode configuration was used with a Pt wire as the counter electrode and a Pt disc as the working electrode. The measured redox potential of Fc^+/Fc was +102 mV vs. ANE compared to the previously reported +87 mV by Pavlishchuk et al[28], who also reported a potential difference of 542 mV between their ANE in acetonitrile and SHE. Thus, we determined that the difference between our ANE electrode and SHE is +557 mV.

DSSC fabrication:

Dye-sensitized TiO_2 solar cells (DSSCs) were fabricated as detailed elsewhere.[29] In brief, a thin compact layer of TiO_2 was deposited on a cleaned fluorine-doped SnO_2 glass substrate (TEC8), using 0.2 M titanium diisopropoxide bis(acetylacetonate) in isopropanol by spray pyrolysis, followed by heating at 450 °C for 30 min. Mesoporous TiO_2 films were deposited via the screen-printing technique using a paste of 22 nm-sized TiO_2 nanoparticles on a TCO

substrate and then sequentially sintered at 325 °C for 5 minutes, 375 °C for 5 minutes, 450 °C for 15 minutes, and 500 °C for 15 minutes. This film was then soaked in 0.04 M $TiCl_4$ solution at 70^{o}C for 30 minutes, rinsed with distilled water, and finally sintered again at 500 °C in air for 30 minutes. This film was then immersed in a solution of acetonitrile and *tert*-butyl alcohol (1:1, v/v) containing 0.5 mM $[RuL_2(NCS)_2]$:2TBA (L = 2,2´-bipyridyl-4,4´-dicarboxylic acid; TBA = tetrabutylammonium; also known as the N719 dye) and 0.5 mM chenodeoxycholic acid (CDCA) for 15 h. Electrolyte was comprised of 1.0 M PMII (1-propyl-3-methylimidazolium iodide), 0.05 M LiI, 0.03 M I_2, 0.5 M *t*BP (4-*tert*-butylpyridine) and 0.1 M GNCS (guanidinium thiocyanate) in a solution of acetonitrile/valeronitrile (85:15, v/v). The average TiO_2 film thickness was about 10 μm as measured with a surface profiler (KLA Tencor Alpha-Step 500).

3. Results and Discussion

3.1. Microstructure and composition of VOG films

Fig. 2 shows SEM images of the three samples (S1, S2, and S3) under two different magnifications to show the surface morphologies. From the inset high magnification images, it can be noticed that all samples consist of quasi-vertically oriented multilayer graphene (MLG) sheets, and the thickness (number of layers) varies from sheet to sheet in the same sample. Some sheets are much thicker, on which thinner sheet are nucleated, and all the sheets form interweaved network. The low magnification images indicate that the nitrogen gas flow ratio during sample growth has great impact on the surface morphology. S1 has a relatively “smooth” surface at a large scale with a lowest sheet density; S2 has a cauliflower-type “particulate” surface with each “particle” consisting of closely packed interconnected sheets; S3 has a “cluster” structure, and in each cluster, there exist a few large (thicker and longer) sheets through which high-density small sheets are connected. These morphologies are similar to the morphologies previously reported by

other groups.[23, 24] SEM cross-sectional images indicate these three samples have a similar average thickness of ~ 30 μm (Fig. S1 in Supplementary Information), giving a growth rate of ~ 1 μm per minute. We want to emphasize that from the film bottom to the top surface, many new branches of graphene sheets can nucleate and grow, and each sheet typically has a thick root and thin top with gradually reduced number of graphene layers, or a tapering shape.

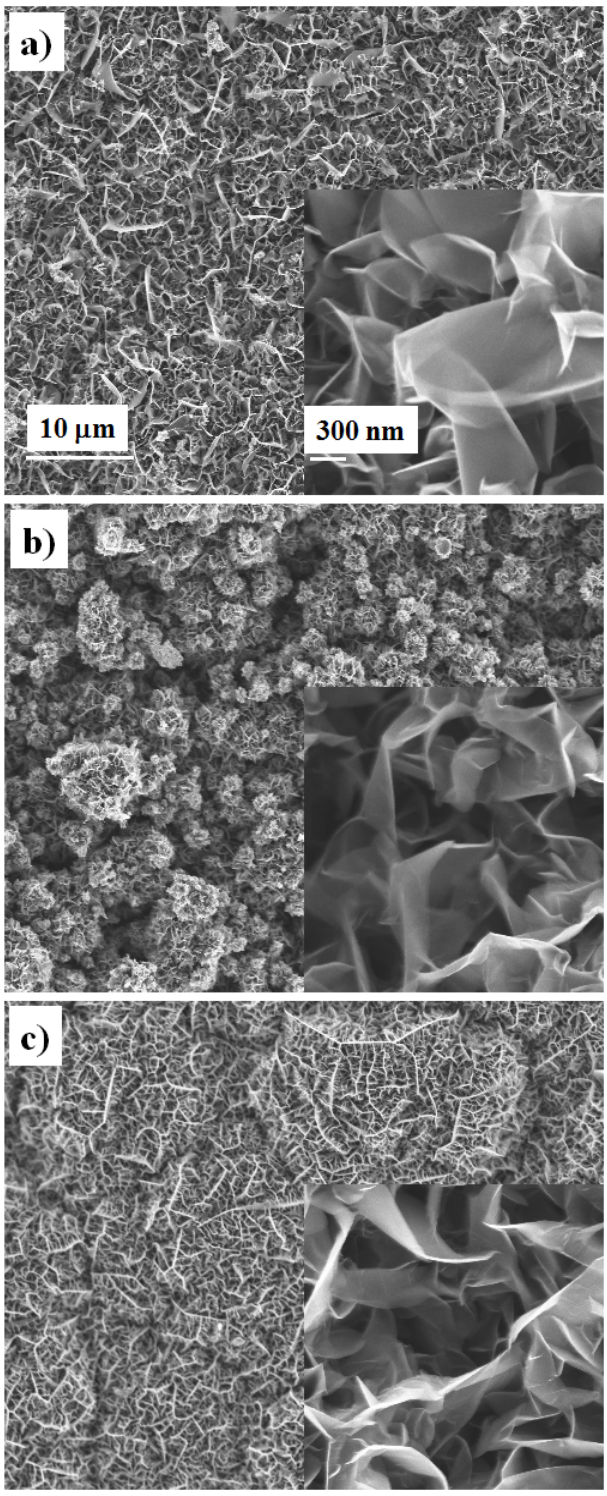

Figure 2 SEM images of three studied VOG samples S1, S2 and S3 acquired at lower and higher (inset) magnifications. The scale bar is the same for a-c).

Although we do not have accurate temperature measurement during VOG growth, the estimation from an optical pyrometer indicates a temperature above 1200 ^{o}C, and the temperature increases as nitrogen flow rate ramps up. The brightness of the plasma also indicates the increase of temperature. Since temperature has significant effect on the crystal quality of carbon graphitization, it is expected that for the three MLG samples of S1, S2, and S3, in addition to the morphology and MLG sheet density difference, their crystal quality could also be different. Raman spectroscopy is commonly used to characterize single and multi-layer graphene sheets. Fig. 3a) presents the Raman spectra of these VOG samples. They were measured under the same conditions using the 514.5 nm line of an argon laser with an excitation laser power of 5mW and an integral time of 5s. They all show the characteristic peaks of graphene at ~ 1352 cm^{-1} (D band), ~ 1586 cm^{-1} (G band), and ~ 2705 cm^{-1} (2D band), in addition to a weak D$'$ peak on the right shoulder of G band. This D$'$ peak, which is attributed to graphene edge effect[30] and typically not obvious for lateral graphene, is discernible for VOG due to the fully exposed graphene edges. Furthermore, this same edge effect causes the D band, the lattice-disorder induced phonon mode, to become obviously stronger than that of the typical lateral graphene. It should be emphasized that unlike for electronic application, when graphene is used for catalytic function, a strong D band does not mean a low performance. In fact, for undoped graphene, a strong catalytic capability is attributed to its edge effect and other defects, and in this sense, stronger D and D′ bands indicate a better catalytic performance. Comparing the spectra of the three samples, they exhibit obvious difference in Raman scattering intensity and the full width at half maximum (FWHM) for their characteristic peaks. It suggests that the overall lattice quality of S3 is the best among these three samples in catalytic function.

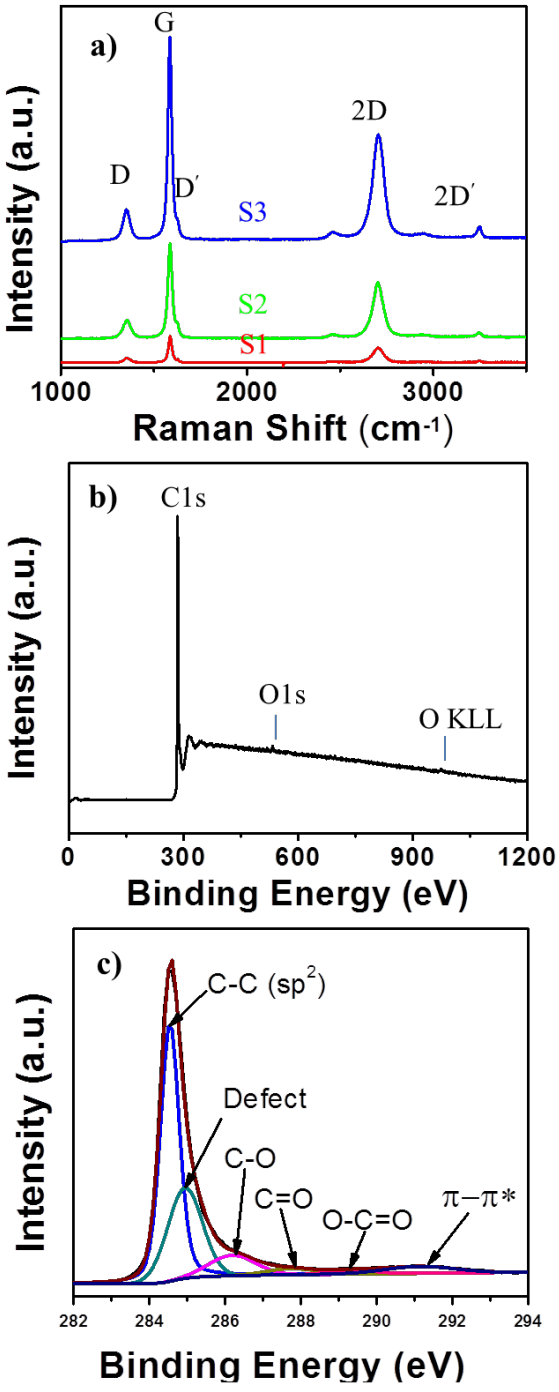

Figure 3 a) Raman spectra of VOG S1, S2 and S3. XPS spectra of S3 as the representative of all VOG samples: b) survey scan, and c) high resolution scan of C1s peak and the related fittings.

Since the aim of this study was to investigate the intrinsic catalytic property of VOG, to avoid the contribution from other functional groups related to heteroatom doping such as oxygen and nitrogen, the chemical composition of these samples was analyzed with X-ray photoelectron spectroscopy (XPS). Considering the detection limit of the instrument, the composition of the three samples was found to be the same with 0.9-1.0 at% oxygen adsorbates on the surface. Fig. 3b) shows the representative XPS survey spectrum, with a strong C 1s peak at 284.6 eV and very weak O1s peak at 532.6 eV, in addition to O KLL Auger band. The high resolution C 1s asymmetric peak is shown in Fig. 3c), in conjunction with peak fitting to identify the different chemical bonds. Based on the common fitting method using Gaussian-Lorentzian function, the C 1s peak can be deconvoluted into six peaks corresponding to sp^2 C-C bond at 284.6 eV, defect at 285.0 eV, C-O bond at 286.6 eV, a weak C=O bond at 288.1 eV, COOH groups at 289.7 eV, and π-π^* shake up at 291.4 eV.[31] In Fig. S2 of the Supplementary Information, the O 1s spectrum is fitted with two Gaussian peaks, corresponding to C-O bond centering at 531.8 eV and C=O bond at 532.9 eV. The chemical bonding analysis is consistent with data in Ref. [[23]]. Two striking points should be emphasized: one is that there is no detectable amount of nitrogen in the samples, even though these samples were grown in a plasma mixture with high concentration of nitrogen, which is not surprising since at such high growth temperature (> 1200^{o}C) the chemical bonds between carbon and nitrogen are not stable, and hence nitrogen cannot be doped into sp^2 carbon lattice;[32] secondly, the oxygen concentration in VOG is trivial. The growth chamber has a base pressure of 1 mtorr, and high purity methane and nitrogen were used as source gases. It is believed that the most of trivial oxygen concentration detected by XPS is due to physical adsorption after exposing samples to the air, and these oxygen impurities probably are electrochemically inert. Therefore, it can be concluded that the electrocatalytic functions of these

VOG samples are their intrinsic capability, not due to heteroatom or other functional groups doping.

3.2. Electron transfer and electrocatalytic study

A facile electron transfer process between an electrode and the electrolyte requires a high density of electrons above Fermi level in the electrode materials that have enough energy to transfer to a close redox pair. It is known that the edge plane of highly oriented pyrolytic graphite has an electrochemical reactivity several orders of magnitude higher than its basal plane due to a large amount of defects at the edge that produce a high density of defect states near the Fermi level. Due to the high density of MLG with fully exposed edges, and further considering that even though some sheets are too thick to be called graphene, their vertically tapering shape reveal many steps or edges of each atomic layers. These atomic edges or steps are the potential adsorption sites of redox species in electrolyte and sites of electron transfer. In addition, plasma bombardment may also introduce a large amount of defects in the basal plane that further enhance the catalytic capability. Therefore, with such morphology and high density of defects at the edge or in the plane, VOG films, even without any heteroatom doping, may also possess useful electrocatalytic capability.

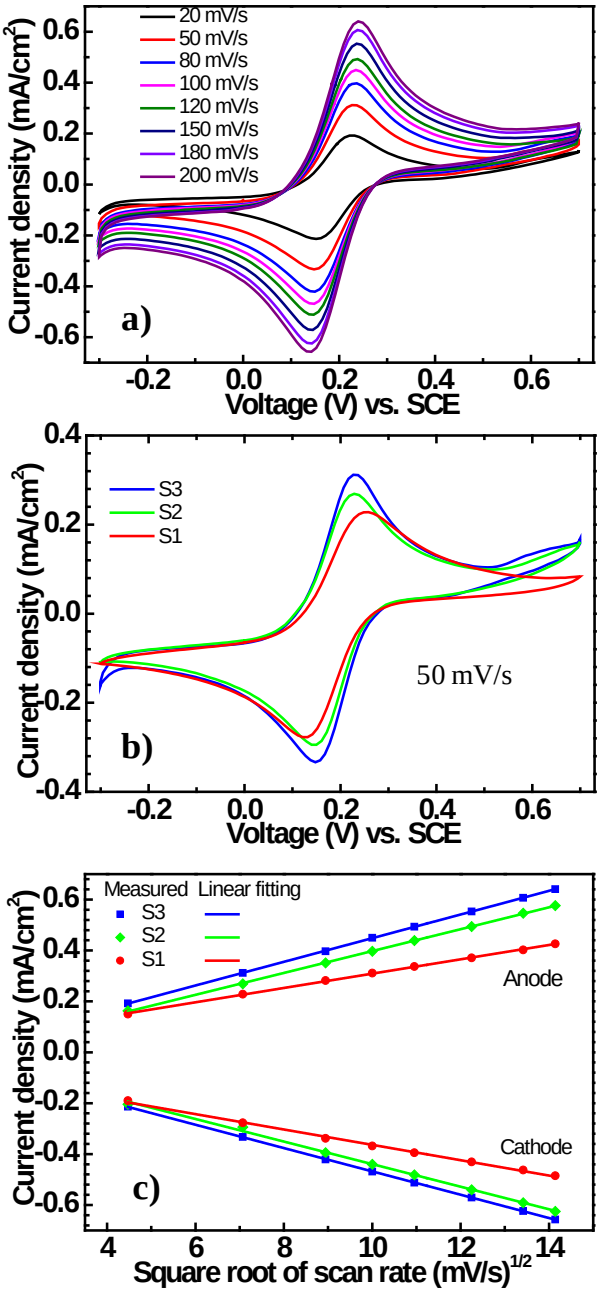

Figure 4 a) Cyclic voltammograms of S3 electrode in 0.25 mM ferrocouple electrolyte with different scan rates from 20-200 mV/s; b) Comparison of C-V profiles of S1, S2 and S3 at the same scan rate of 50 mV/s; c) Anodic and cathodic peak current density as a function of the square root of scan rates for S1, S2 and S3.

The electron-transfer reaction between VOG films and electrolyte were investigated by cyclic voltammetry in an electrolyte of 0.1 M KCl aqueous solution containing 0.25 mM $K_3[Fe(CN)_6]$ / $K_4[Fe(CN)_6]$ (1:1). $Fe(CN)_6^{3-/4-}$ redox couple was used since it has been extensively employed to study the electron transfer dynamics of different carbon allotropes, including graphene. Fig. 4a) presents the cyclic-voltammetric (C-V) of VOG S3 at different scan rates from 20 to 200 mV/s (the C-V profiles for S1 and S2 are plotted in Fig. S3 of the Supplementary Information). Fig 4b) compares the C-V profiles of these three samples at the scan rate of 50 mV/s. The electrochemical measurements indicate that all the samples exhibit perfect reversible response, a characteristic of VOG electrodes with rapid electron-transfer kinetics; however, the reduction and oxidation peak-to-peak separation (E_{pp}) of these samples is different. For S1, E_{pp} is in the range between 108 mV to 189 mV, while for both S2 and S3, this value is similar, from 70 mV to 100 mV, depending on the scan rate. Fig. 4c) shows the anodic and catholic current density as a function of the square root of scan rate for the three samples, with S3 displaying the highest current density. The obtained linear relationship between the current density of electrodes and the square root of the scan rate is in agreement with the modified Cottrell equation ($j=k\,s^{1/2}$, where s is the scan rate, and k is the collection constant determined by the electrochemical system), which provides evidence for the diffusion controlled electrochemical reaction and fast electron transfer at the interface between the electrode and electrolyte. Our measured small values of E_{pp}, especially for S2 and S3 at low scan rates, reveal that these samples can provide facile electron transfer to and from the electrolyte. This is because in this single-electron Nerstian process with the reaction rate controlled by the electrolyte diffusion, E_{pp} is correlated with the electron transfer coefficient, and single-electron reaction has an ideal value of 59 mV. As emphasized above, these VOG samples have no heteroatom

functionalization, and their electrocatalytic capability is due to the large density of fully exposed graphene edges and in-plane defects. On the other hand, the physical property differences in morphology, graphene sheet density, and crystalline quality of the three samples, due to the growth condition variation, are accompanied by electrocatalytic performance disparity, reflected by peak-to-peak potential separation and electrode current density. These electron transfer dynamic study results suggest that S3 would be the best counter electrode for DSSC for I^-/ I_3^- reduction, and S1 would be comparatively the worst counter electrode.

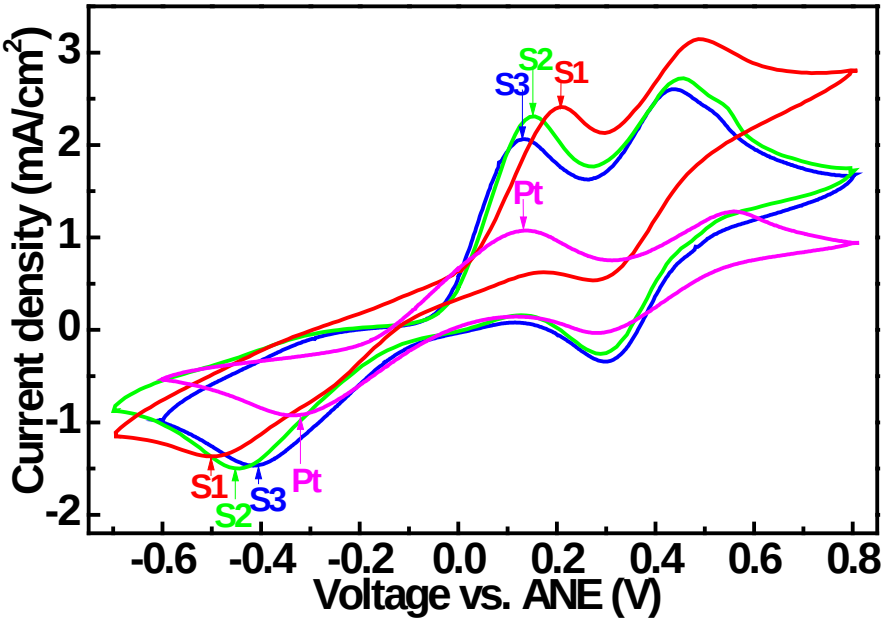

Figure 5 Cyclic voltammograms of S1, S2 and S3 in acetonitrile solution containing 0.1 M $LiClO_4$, 5 mM LiI, and 0.5 mM I_2 at scan rate of 50 mV/s. The C-V profile of a platinized FTO electrode is also plotted as reference.

This is confirmed by the I^-/ I_3^- redox reaction study. To investigate the electrocatalytic activity of VOG electrode on I^-/ I_3^- redox couple, cyclic voltammogram of each VOG electrode

was measured in acetonitrile solution containing 10 mM LiI, 1 mM I_2 and 0.1 M $LiClO_4$. This solution has a much lower concentration than the typically used electrolyte of DSSC to clearly resolve the redox peaks. Three-electrode configuration was employed for this measurement with Pt wire as the counter electrode and non-aqueous Ag/Ag^+ reference electrode (ANE) as the reference electrode. Fig. 5 presents the C-V profiles of VOG electrode for I^-/ I_3^- redox study. In addition to the three VOG samples, the platinized FTO electrode that is commonly used as counter electrode of DSSC is also measured for comparison. Two pairs of redox peaks were observed for all samples. The relative positive and negative pairs can be assigned to the oxidation and reduction of I_2/ I_3^- and I_3^-/ I^- respectively.[14, 19] Since the reduction of I_3^- to I^- is the actual reaction occurring at the counter electrode in a DSSC, our analysis is focused on the negative pairs. The peak to peak separation (E_{pp}) for the three VOG electrodes of S1, S2 and S3 were found to be 708 mV, 599 mW, and 552 mV, respectively, indicating that the electrocatalytic capability of S3 was the best. This is in consistence with the above electron-transfer dynamic study results. However, the E_{pp} value of S3 (552 mV) is still higher than that of the platinized FTO electrode (477 mV), suggesting a relatively lower redox reaction rate by comparing VOG with platinized FTO. On the other hand, the porous structure of VOG samples gives them much larger apparent surface area and active catalytic sites, leading to a higher current density than the platinized FTO electrode.

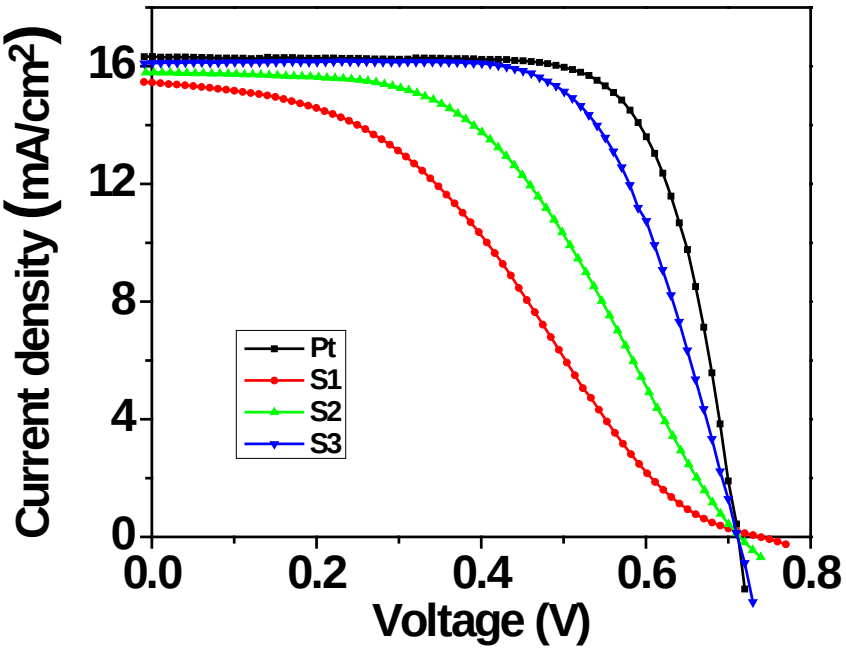

Figure 6 Comparison of *J–V* characteristics of dye-sensitized solar cells using the standard Pt and VOG S1, S2 and S3 counter electrodes.

Table 1. Effect of the counter electrode material on the short-circuit photocurrent density J_{sc}, open-circuit voltage V_{oc}, fill factor FF, and conversion efficiency η of dye-sensitized solar cells.

Counter Electrode Type	J_{sc} (mA/cm^2)	V_{oc} (V)	FF	η (%)
S1	15.45	0.739	0.365	4.17
S2	15.79	0.715	0.494	5.58
S3	16.11	0.712	0.665	7.63
Pt	16.33	0.711	0.730	8.48

3.3. DSSC characterization

We examined the effectiveness of using VOG as counter electrodes for dye-sensitized solar cells (DSSCs). Fig. 6 shows the photocurrent-voltage (*J–V*) characteristics of DSSCs based

on different VOG samples (S1, S2 and S3). The *J–V* characteristic of a standard DSSC using Pt counter electrode is also shown as a reference for comparison. The details of the photovoltaic parameters (J_{sc}, V_{oc}, FF, and η) for all these cells are given in Table 1. When S1 was used as a counter electrode, the cell displayed an efficiency of 4.17% with fill factor of 0.365. The cell performance improved from 4.17% (S1) to 5.58% (S2) to 7.63% (S3), resulting primarily from an improved fill factor from 0.365 (S1) to 0.494 (S2) to 0.665 (S3). As shown in Table 1, the device performance of the best, S3-based, cell is slightly inferior to that of the Pt-based DSSC. The increase of fill factor is consistent with the better catalytic properties of different VOG samples as shown and discussed above.

Electrochemical impedance spectroscopy (EIS) measurements were conducted to understand the effect of different counter electrodes on the charge transfer kinetics at the counter electrode. Fig. S4 in Supplementary Information shows the typical impedance spectra of VOG-based DSSC measured at two different bias voltages at open circuit under illumination. From EIS study, two features of the impedance response can be identified: (1) a large semicircle at low frequencies (approximately <10 Hz), which corresponds to the back charge-transfer process at TiO_2/redox electrolyte interface with a recombination resistance R_{ct}; and (2) a small semicircle at high frequencies (approximately >30 Hz), which is associated with the charge-transfer process at the counter electrode/electrolyte interface with a charge-transfer resistance R_p. Normally, there is a linear region with 45^o slope at medium frequencies, which is characteristic for the transmission line model and can be used to derive the transport resistance of the TiO_2 electrode. However, this feature is not obvious in the current study. This would not affect our understanding on the charge transfer kinetics at the counter electrode/electrolyte interface. It is evident that R_{ct} decreases with increasing bias voltage, which is in agreement with the results of previous studies.[33] In contrast,

the small semicircle associated with charge-transfer at the counter electrode does not change significantly with the bias voltage. Analysis of the impedance spectra indicates that the R_p value decreases from about 153 Ω to 81 Ω to 53 Ω for the three samples S1-3. Smaller charge-transfer resistance corresponds to a faster kinetics. These impedance results are consistent with the impact of nitrogen flow rate on the morphological changes and electrochemical studies of the VOG films as discussed above.

4. Conclusions

This study demonstrated that VOG films grown by PECVD at high temperature, with their fully-exposed graphene edges that produce a high density of defect states, in addition to the in-plane defects, exhibits superior intrinsic electrocatalytic properties. Comparative studies found that as growth temperature increased due to nitrogen ratio increase in the source gas, the structure and electrocatalytic properties of VOG changed. Electron transfer dynamics measurement found that VOG electrodes can provide rapid electron-transfer kinetics, while the electrocatalytic activity study indicated that the reduction activity of VOG on I^-/ I_3^- redox couple can approach that of platinum. Using VOG as counter electrodes for DSSCs, a power conversion efficiency of 7.63% was demonstrated. This study suggested that VOG has the potential as a promising electrocatalyst to replace Pt for DSSC and other applications.

K.Z. acknowledges the support by the Division of Chemical Sciences, Geosciences, and Biosciences, Office of Basic Energy Sciences, U.S. Department of Energy, under contract No. DE-AC36-08GO28308 with the National Renewable Energy Laboratory

References:

1. B. Oregan and M. Gratzel, *Nature*, 1991, **353**, 737-740.
2. A. Hagfeldt, G. Boschloo, L. Sun, L. Kloo and H. Pettersson, *Chem. Rev.*, 2010, **110**, 6595-6663.
3. K. Zhu, N. R. Neale, A. Miedaner and A. J. Frank, *Nano Lett.*, 2007, **7**, 69-74.
4. Y. Li, H. Wang, Q. Feng, G. Zhou and Z.-S. Wang, *Energy Environ. Sci.*, 2013, **6**, 2156-2165.
5. X. Pan, C. Chen, K. Zhu and Z. Fan, *Nanotechnology*, 2011, **22**, 235402.
6. J. Liu, Y.-T. Kuo, K. J. Klabunde, C. Rochford, J. Wu and J. Li, *ACS Appl. Mater. Inter.*, 2009, **1**, 1645-1649.
7. Y. Alivov and Z. Y. Fan, *J. Mater. Sci.*, 2010, **45**, 2902-2906.
8. Z. Yang, S. Gao, W. Li, V. Vlasko-Vlasov, U. Welp, W.-K. Kwok and T. Xu, *ACS Appl. Mater. Inter.*, 2011, **3**, 1101-1108.
9. Z. Huang, X. Liu, K. Li, D. Li, Y. Luo, H. Li, W. Song, L. Chen and Q. Meng, *Electrochem. Comm.*, 2007, **9**, 596-598.
10. K. Imoto, K. Takahashi, T. Yamaguchi, T. Komura, J.-I. Nakamura and K. Murata, *Sol. Energ. Mat. Sol. Cells*, 2003, **79**, 459-469.
11. W. J. Lee, E. Ramasamy, D. Y. Lee and J. S. Song, *ACS Appl. Mater. Inter.*, 2009, **1**, 1145-1149.
12. C.-T. Hsieh, B.-H. Yang and J.-Y. Lin, *Carbon*, 2011, **49**, 3092-3097.
13. H. Wang and Y. H. Hu, *Energy Environ. Sci.*, **5**, 8182-8188.
14. J. D. Roy-Mayhew, D. J. Bozym, C. Punckt and I. A. Aksay, *ACS Nano*, 2010, **4**, 6203-6211.
15. D. W. Zhang, X. D. Li, H. B. Li, S. Chen, Z. Sun, X. J. Yin and S. M. Huang, *Carbon*, 2011, **49**, 5382-5388.
16. X. Pan, Y. Zhao, S. Liu, C. L. Korzeniewski, S. Wang and Z. Fan, *ACS Appl. Mater. Inter.*, 2012, **4**, 3944-3950.
17. X. Xu, D. Huang, K. Cao, M. Wang, S. M. Zakeeruddin and M. Gratzel, *Sci. Rep.*, 2013, **3**, 1489.
18. J.-S. Lee, H.-J. Ahn, J.-C. Yoon and J.-H. Jang, *Phys. Chem. Chem. Phys.*, 2012, **14**, 7938-7943.
19. Y. Xue, J. Liu, H. Chen, R. Wang, D. Li, J. Qu and L. Dai, , *Angew. Chem.Inter.Ed.*, 2012, **51**, 12124-12127.
20. S. Hou, X. Cai, H. Wu, X. Yu, M. Peng, K. Yan and D. Zou, *Energy Environ. Sci.*, 2013, **6**, 3356-3362.
21. W.-Y. Cheng, C.-C. Wang and S.-Y. Lu, *Carbon*, 2013, **54**, 291-299.
22. H. Wang, K. Sun, F. Tao, D. J. Stacchiola and Y. H. Hu, *Angew. Chem.Inter.Ed.*, 2013, **52**, 9210-9214.
23. N. G. Shang, P. Papakonstantinou, M. McMullan, M. Chu, A. Stamboulis, A. Potenza, S. S. Dhesi and H. Marchetto, *Adv. Func. Mater.*, 2008, **18**, 3506-3514.
24. M. Cai, R. A. Outlaw, S. M. Butler and J. R. Miller, *Carbon*, 2012, **50**, 5481-5488.
25. G. Ren, X. Pan, S. Bayne and Z. Fan, *Carbon*, 2014, **71**, 94-101.
26. H. Fang, C. Yu, T. Ma and J. Qiu, *Chem. Comm.*, 2014, **50**, 3328-3330.
27. M. J. Ju, J. C. Kim, H.-J. Choi, I. T. Choi, S. G. Kim, K. Lim, J. Ko, J.-J. Lee, I.-Y. Jeon and J.-B. Baek, *ACS Nano*, 2013, **7**, 5243-5250.

28. V. V. Pavlishchuk and A. W. Addison, *Inorg. Chim. Acta*, 2000, **298**, 97-102.
29. N. R. Neale, N. Kopidakis, J. van de Lagemaat, M. Gratzel and A. J. Frank, *J. Phys.Chem. B*, 2005, **109**, 23183-23189.
30. A. C. Ferrari, *Solid State Comm.*, 2007, **143**, 47-57.
31. M. Beidaghi and C. Wang, *Adv. Func. Mater.s*, 2012, **22**, 4501-4510.
32. H. Wang, T. Maiyalagan and X. Wang, *ACS Catalysis*, 2012, **2**, 781-794.
33. K. Zhu, S.-R. Jang and A. J. Frank, *J. Phys. Chem. Lett.*, 2011, **2**, 1070-1076.

Table of contents entry

Vertically oriented graphene exhibits meritorious electrocatalytic properties due to exposed graphene edges and other defects, even without any heteroatom functionalization.